NANO LETTERS

pubs.acs.org/NanoLett Letter

Neutron Scattering Reveals a Dynamic Surface Equilibrium on L-α-Lecithin Functionalized $CsPbBr_3$ Nanocrystals

Jan Wahl, Ivan Zaluzhnyy, Sylvain Prevost, Lionel Porcar, Christian Beck, Olga Matsarskaia, Tobias Unruh, Ezzeldin Metwalli, Frank Schreiber, Marcus Scheele, and Tilo Seydel*

Cite This: *Nano Lett.* 2026, 26, 8208−8216 Read Online

ACCESS | Metrics & More | Article Recommendations | Supporting Information

ABSTRACT: Cesium lead bromide perovskite nanocrystals (NCs) covered with lecithin ligands in liquid toluene suspensions were investigated with a range of complementary scattering techniques and nuclear magnetic resonance to reveal their surface chemistry, solution structure, and diffusive dynamics. Distinct self-diffusion coefficients were determined and analyzed, namely the center-of-mass diffusion of the NCs and of coexisting ligand micelles, as well as the lateral diffusion of the L-α-lecithin ligand relative to the NC surface and within the micelles. We find a dynamic surface equilibrium, represented by a tunable lateral diffusion coefficient dependent on the ligand surface density. This phenomenon can be rationalized by the extraordinary binding of this zwitterionic ligand and its ability to bind via two different binding sites. These results highlight the dynamic nature of the ligand binding to lead halide perovskite NCs.

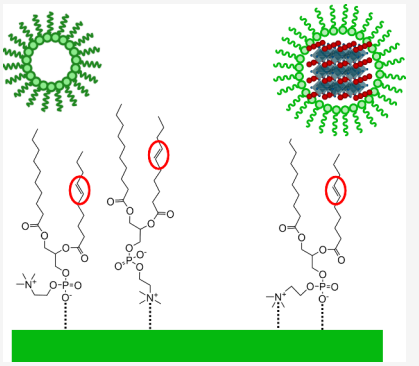

KEYWORDS: *Perovskites, Ligand Dynamics, Neutron Scattering, High-resolution Neutron Spectroscopy, Nuclear Magnetic Resonance, Small Angle Scattering*

Lead halide perovskite (LHP) nanocrystals (NCs) are promising for the application in novel optoelectronic devices.[1−3] Besides the LHP itself, the organic ligand shell of the NCs is crucial in this respect.[4,5] For instance, the quantum yield (QY) of LHP NCs can be tuned by the choice of ligand shells.[6−8] In light-emitting diodes, this effect as well as the equally ligand-dependent charge injection barrier are exploited to enhance the performance of LHP NC-based devices.[9,10] One of the major drawbacks of LHP NCs, their limited stability, can also be tailored by the ligand shell. By utilizing proper ligands and fine-tuning the surface ligand density, the stability of LHP-based NCs was shown to increase largely.[6,11,12] Chemical modifications of the ligand shell are either carried out in situ or by postsynthetic treatment.[9] Especially the latter case is advantageous for optoelectronic applications, as the ligands can be selected to fit specific needs without developing novel synthesis routes.[9] The rational design of these ligand exchange procedures requires detailed knowledge of the NC surface chemistry and ligand molecule dynamics.[13]

Here, we study the surface chemistry of L-α-lecithin covered all-inorganic $CsPbBr_3$ NCs in deuterated toluene and reveal a dynamic surface equilibrium. To this end, we combine results from Nuclear Magnetic Resonance (NMR), which probes angular correlations,[14,15] with simultaneous X-ray and neutron small-angle scattering (SAXS and SANS) for probing spatial correlations on a mesoscopic scale, as well as quasi-elastic neutron spectroscopy (QENS), accessing both spatial and temporal correlations simultaneously on a scale commensurate with molecule dimensions.[16] These methods are well suited for optically opaque liquid samples, where other techniques relying on optical transmission would fail. The present work benefits from a novel simultaneous SAXS and SANS setup[17] as well as from a novel inverted neutron time-of-flight backscattering spectrometer denoted BATS.[18−20] QENS on our samples exploits the dominant incoherent scattering signal of the lecithin ligands against the deuterated solvent background in the investigated range in momentum transfer $\hbar q$ and energy transfer $\hbar\omega$. It, thus, probes the self-diffusion of the ligands in their different configurations, i.e., on the NCs, free, or inside lecithin micelles, respectively. Due to the nanosecond coherence time of the QENS experiment, this self-diffusion is observed on the diffusive short-time scale on which the NCs displace by only a small fraction of their radius. On this scale, collisions between the NCs can be neglected, and the center-of-mass diffusion can be assumed to be governed by hydrodynamic interactions. Due to the large q accessed, the QENS experiment simultaneously probes both the lateral

Received: March 25, 2026
Revised: June 13, 2026
Accepted: June 15, 2026
Published: June 19, 2026

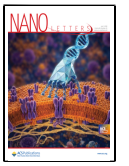

https://doi.org/10.1021/acs.nanolett.6c01347
Nano Lett. 2026, 26, 8208−8216

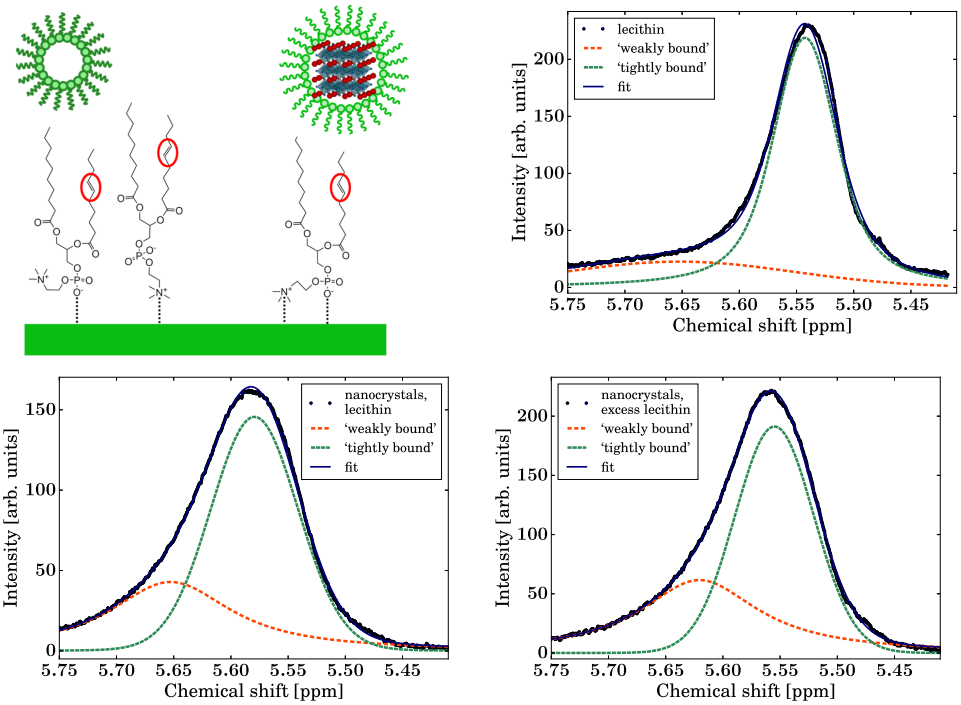

Figure 1. Top left: Model of the surface chemistry of lecithin on $CsPbBr_3$ NCs: Top part: Schematic of a NC decorated by lecithin (right) and of a coexisting reverse micelle formed from lecithin (left). Bottom part: cartoon of the binding of the zwitterionic lecithin lipid ligands on the NC surface, with the bonds between NC and ligand shown as dotted lines, and truncated lipid tails. The bonds may be single with either of the ions (left) or double (right). The NMR spectra (top left and bottom row plots) probe the protons in the alkene regions (red ellipses on the lecithin chemical structures). Top right and bottom left and right: NMR spectra of the lecithin alkene region (5.4−5.7 ppm) with fits using Voigt functions of the lecithin reference, as-synthesized NCs and the excess ligand sample. The legends assign the samples and the fit parameters are summarized in Table S2.

diffusion of the lecithin, as well as the superimposed center-of-mass diffusion of the ligand-decorated micelles and NCs.[21] The QENS experiment also accesses a wide sample temperature T range. The large energy range investigated combined with the good energy resolution of 3.5 μeV fwhm of BATS allows to unambiguously separate the apparent global diffusion from the faster diffusive processes within the ligand shell. NMR as well as the scattering methods (SAXS, SANS and QENS) access ensemble-averaged signals from the complex samples consisting of the decorated nanocrystals and of coexisting lecithin not attached to the NCs in the toluene solution. By applying these methods to the identical same samples and by combining the results, we obtain a consistent picture of this dynamic coexistence. We interpret the results based on the coexistence of lecithin on the NC surface and inside reverse micelles, as confirmed by SAXS/SANS and agreeing with the other methods.

The as-synthesized NCs covered by L-α-lecithin exhibit an onset of absorption at 510 nm in the ultraviolet-to-visible light spectrum (UV−vis) and a corresponding photoluminescence (PL) signal centered at 513 nm (Figure S1a). Scanning electron microscopy (SEM) reveals an average radius of (4.2 ± 0.6)nm (Figure S1b,c) in good agreement with a radius of ∼4.5nm inferred from the PL peak position.[22,23]

We characterize the ligand shell by ^{1}H NMR on an as-synthesized NC sample with lecithin, a lecithin reference, and an NC sample with added excess lecithin (see Materials and Methods and the Supporting Information (SI) for a description of all samples). L-α-Lecithin exhibits a characteristic ^{1}H NMR signal at ≈5.5ppm associated with alkene protons (Figure 1 and Figures S2 and S3), which we model by a sum of peaks to account for its asymmetry suggesting the presence of multiple ligand species (cf. Figure 1 top left). The assignment of these fitted peaks follows similar considerations previously reported for the oleic acid alkene peak in decorated colloidal NC samples.[24−26] In this context, a downfield shift in NMR of colloidal NC samples can often be attributed to ligand molecules in proximity to either NCs or other ligand molecules, i.e., bound to the NC surface or attached in a micelle.[26] In general, chemical shifts are described by Lorentzian functions (cf. eq 1) in the case of liquid samples under ideal conditions, with additional Gaussian contributions arising from random broadening.[27] Therefore, we fitted the chemical shifts in the region attributed to alkene by a sum of Voigt functions in terms of the chemical shift peak position x, amplitude, Lorentzian width γ, and Gaussian width σ (Figure 1, Table S2).[27,28] γ is inversely proportional to the spin−spin relaxation time T_2, and thus, in the simplest picture of rigid spherical molecules, proportional to the rotational diffusion.[29,30] A broader or more heterogeneous NMR signal can in some cases be associated with geometrically confined motions, cf. ref[30] and references therein.

We obtain stable fits with two Voigt profiles for each NMR spectrum (Figure 1, Table S2), showing similar peak positions for all samples, without imposing that position in the fit. We find a strong Gaussian broadening of the peak at the higher chemical shift for the pure lecithin sample, as well as for the peak at the lower shift for the samples containing NCs. For the Lorentzian broadening, this behavior is inverted, i.e., the pure lecithin sample shows a strong Lorentzian broadening of the lower-shift peak, and the NC samples display a strong Lorentzian broadening of the higher-shift peak. The relative

https://doi.org/10.1021/acs.nanolett.6c01347
Nano Lett. 2026, 26, 8208−8216

intensity of the lower-shift peak decreases in the presence of the NCs.

We tentatively intrepret these trends as follows: Stronger hydrogen bonds in some cases can be attributed to more delocalized structures resulting in downfield NMR chemical shifts compared to weaker bonds.[31] Accordingly, we attribute the two peaks to "tightly bound" and "weakly bound" (Table S2), respectively, but stress that these attributes are relative and do not imply a weak bonding in absolute terms. In this assignment, the stronger weight of the Lorentzian term in weakly bound lecithin indicates more fluid-like behavior of this population in the presence of the NCs, combined with a larger relative area in the spectrum. Conversely, the strongly bound lecithin is Lorentzian, i.e., fluid-like in the pure lecithin sample and Gaussian-like, i.e., dynamically heterogeneous, in the presence of the NCs, while also taking a stronger spectral weight in the presence of the NCs. Thus, the fraction of lecithin covering the NCs may strongly contribute to this signal, but part of this signal also seems to arise from lecithin bound in the micelles. Limitations to this interpretation arise from the missing link between the microsecond relaxation dynamical information from this NMR experiment and the associated spatial correlations. Importantly, the ^{1}H NMR chemical shifts only inform on changing relative weights, but not on absolute fractions of dynamical contributions. In contrast, possible oleate contaminations from the sample preparation can be ruled out due to their distinctly different shifts.[32]

Reverse micelles can be expected in nonpolar solvents.[33,34] We measured lecithin in deuterated toluene from very dilute up to the typical lecithin concentration in the presence of the nanocrystals, to assess the existence of such self-assembled structures. Data presented in the SI (Figure S4) together with fits assuming homogeneous polydisperse spheres show the absence of visble dissociation in the measured range, i.e., these concentrations are above the critical micelle concentration. The micelle radius of 3.0 nm determined by SANS agrees well with the hydrodynamic radius $R_{h,\mathrm{LE}}$ = 2.5 nm obtained from QENS (see further below), and with literature.[35,36]

Figure 2 depicts simultaneously acquired SANS and SAXS data for $CsPbBr_3$ NC with lecithin in d-toluene. The differing intensities result from the sensitivity of the methods toward the inorganic core and organic ligand shell.[21,37,38] While SAXS is mostly sensitive to heavy atoms, the SANS signal originates predominantly from the contrast between hydrogen atoms in the ligand (low scattering length density SLD) and deuterium atoms from the solvent (high SLD).[21,38] SANS and SAXS data of the NC dispersions and SANS data of the pure lecithin in d-toluene were fitted simultaneously with a simple model involving two contributions: one for polydisperse homogeneous spheres (reverse micelles of lecithin) and one for core−shell spheres of distributed core radius and uniform shell thickness (ligand-coated nanoparticles) (Figure 2). The fits indicate a satisfactory model and support the hypothesis that two populations are in equilibrium, with lecithin-stabilized NCs (core radius (5.05 ± 1.01)nm, shell thickness (1.3 ± 0.26)nm) coexisting with an excess of micelles (radius (3.02 ± 0.31)nm). The best fits indicate either a rather small shell thickness compared to the micellar radius and the expected length of a lecithin molecule or, most likely, a weaker contrast between shell and solvent than expected for a full coverage. We note that the ligand shell on the NCs contributes to the scattering intensity in a similar q-range as the micelles,

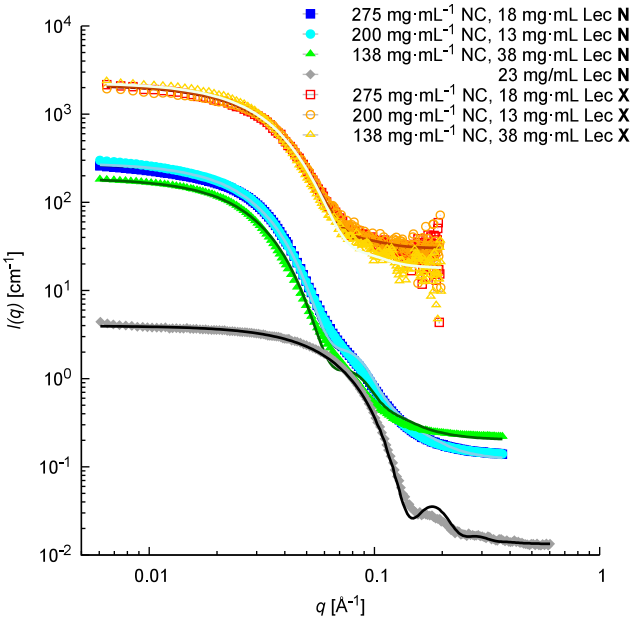

Figure 2. SANS (legend entries marked with "N") and SAXS (legend entries marked with "X") curves recorded simultaneously using D22 (ILL) on $CsPbBr_3$ with lecithin in d_8-toluene (symbols), with simultaneous fits of the corresponding X-ray and neutron curves (continuous lines).

resulting in ambiguity between micellized lecithin and adsorbed lecithin (Figure S6).

The relatively low surface coverage by lecithin consistent with other studies[22,28] found by the simultaneous SAXS/SANS fits can be related to the scattering at low q (Figure S5), pointing to different interaction potentials between NCs, and an upturn at the lowest q in line with the limited solubility of the dispersion. The equilibrium of lecithin between NCs and micelles results in a complex interplay, as a deficiency in ligands will result in aggregation of NCs but an excess of micelles might induce depletion interactions leading to NC aggregation.[39]

To complement the steady-state information obtained from NMR and SAXS/SANS with information on NC surface dynamics, we conduct QENS. By employing deuterated toluene as a solvent, but protonated ligands, the QENS experiment is sensitive to the dominant nuclear spin-incoherent scattering by the ligand protons. In this way, we probe the self-diffusion of the ligand molecules within the observation time window from on the order of 10 ps to 1 ns (cf. Materials and Methods). We assume a superposition of dynamic contributions from the center-of-mass diffusion D of the NCs as well as the lateral diffusion of the ligand D_{jump}. Due to the coexistence of lecithin on NCs and in micelles concluded from the SAXS/SANS experiment, we further assume distinct center-of-mass and lateral diffusion coefficients for each of these two populations. Moreover, we account for the signal from the d8-toluene solvent. Thus, our model consists of a weighted sum of Lorentzian functions

$$\mathcal{L}_{\gamma_i}(q) = \frac{\gamma_i(q)}{\pi}\frac{1}{\gamma_i(q)^2 + \omega^2} \tag{1}$$

where $\gamma_i(q)$ denotes the line width (half-width at half-maximum) and ω the frequency associated with the energy transfer $\hbar\omega$. We fit the complete model, eq 2, simultaneously

https://doi.org/10.1021/acs.nanolett.6c01347
Nano Lett. 2026, 26, 8208−8216

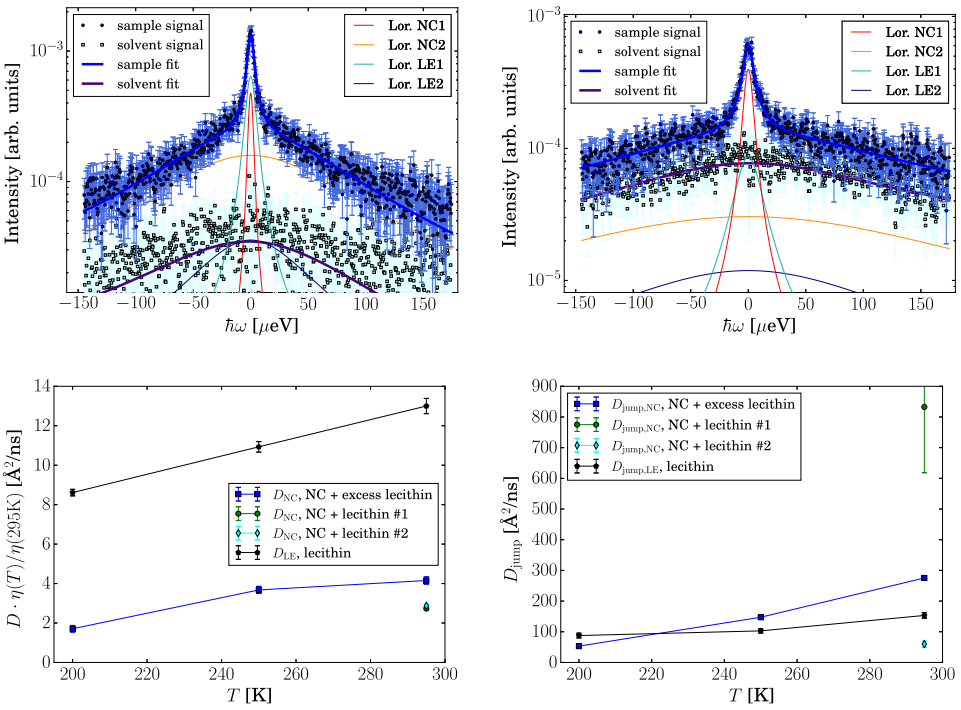

Figure 3. QENS results: Top row: Example spectra at T = 295 K, q = 0.7Å^{-1} (left) and q = 1.2Å^{-1} (right) with fits by eq 2 with Lorentzians $\mathcal{L}_x$ with $x \in$ {NC1, NC2, LE1, LE2} (thin solid lines) as assigned in the legend and described in the main text. Dark circles denote the NC+excess lecithin sample, light squares the pure d-toluene solvent. The thick solid lines on the sample and solvent spectra represent the respective total fits. The fitted container contribution was subtracted after fitting. Data were binned for better visibility. Bottom left: Fit results for the center-of-mass diffusion D of reverse micelles in the pure lecithin reference (black), the as-synthesized NCs with lecithin (green and cyan, "lecithin #1" and "#2"), and the excess ligand NC (blue) samples at different T, rescaled by d-toluene viscosity η from literature (cf. Materials and Methods for sample characteristics, Figure S7 for $\eta(T)$). Bottom right: Lateral diffusion D_{jump} (eq 3) relative to the NCs and micelles, respectively, for all samples as in the bottom left, but without scaling for η. (The apparent outlier for D_{jump} in "lecithin #1" may be attributed to a weak signal amplitude.) The error bars on the fit parameters report 2σ confidence from the diagonal of the covariance matrix, being often smaller than the symbols due to the global fit.

for all q, i.e., two-dimensionally over q and ω, as explained in more detail in the SI,

$$S(q,\omega) = \beta(q)\cdot\{r[A_0(q)\mathcal{L}_{\gamma_{\mathrm{NC1}}}(q) + (1 - A_0(q))\mathcal{L}_{\Gamma_{\mathrm{NC2}}}(q)] + (1 - r)[A_1(q)\mathcal{L}_{\gamma_{\mathrm{LE1}}}(q) + (1 - A_1(q))\mathcal{L}_{\Gamma_{\mathrm{LE2}}}(q)]\} + \beta_{\mathrm{Tol}}(q)\mathcal{L}_{\gamma_{\mathrm{Tol}}}(q) \quad (2)$$

where $\beta(q)$ and $\beta_{\mathrm{Tol}}(q)$ denote the intensity scaling factors for the combined NC and lecithin signals and the d-toluene signal, respectively. $\beta_{\mathrm{Tol}}(q)\mathcal{L}_{\gamma_{\mathrm{Tol}}}(q)$ is obtained from the fits of the pure d-toluene spectra and subsequently fixed, accounting for the volume excluded by the lecithin and NCs. The Lorentzian $\mathcal{L}_{\gamma_{\mathrm{LE1}}}(q)$ accounts for lecithin micelle center-of-mass diffusion and $\mathcal{L}_{\gamma_{\mathrm{LE2}}}(q)$ for the diffusion of the lecithin within the micelle, i.e., the above-mentioned lateral diffusion. $\mathcal{L}_{\gamma_{\mathrm{NC1}}}(q)$ represents the center-of-mass diffusion of the lecithin-decorated NCs and $\mathcal{L}_{\gamma_{\mathrm{NC2}}}(q)$ the diffusion of the lecithin relative to the NC. The scalar fit parameter r denotes the ratio between lecithin in micelles and lecithin on NCs. $A_0(q)$ and $A_1(q)$ describe the relative weight of the center-of-mass diffusion of the NCs and the micelles, and of the lateral diffusion of the lecithin relative to the NC surfaces and to the micelles, respectively. Consistent with the colloidal stability of the NCs shown by our SANS experiment and literature,[40] we impose a Fickian center-of-mass diffusion for both the lecithin micelles and the lecithin-decorated NCs, i.e., $\gamma_{\mathrm{LE}}(q) = D_{\mathrm{LE}}q^2$ and $\gamma_{\mathrm{NC}}(q) = D_{\mathrm{NC}}q^2$, respectively. Moreover, as for liquids,[41] lipids diffusing in vesicle membranes[42−44] and earlier evidence for other decorated NCs,[21] we impose one so-called jump diffusion process[45] each for the lateral diffusion of the lecithin relative to the NCs and relative to the micelles

$$\Gamma_{\mathrm{NC,LE}}(q) = \frac{D_{\mathrm{jump,NC,LE}}q^2}{1 + D_{\mathrm{jump,NC,LE}}q^2\tau_{\mathrm{NC,LE}}} \quad (3)$$

We assume this lateral diffusion to occur along the NC and micelle surfaces, but it could also reflect dissociation dynamics from the surfaces.

Using eq 2, we obtain excellent fits as illustrated in Figure 3 (top row) and Figure S8. The model eq 2 is justified by NMR and SAXS/SANS that confirm the simultaneous presence of lecithin on micelles and on NCs, as well as the existence of two dynamic populations of lecithin. We report the fit of an alternative simpler model in the SI, which we judge insufficient. We thus obtain separate center-of-mass diffusion coefficients D_{LE} of lecithin micelles and D_{NC} of NCs decorated with lecithin (Figure 3, bottom left). Note the y-axis rescaled by the temperature-dependent d-toluene viscosity $\eta(T)$[46−48] (cf. Figure S7). In this normalization, it becomes evident that D_{LE} follows the Stokes−Einstein relation,[49] which for the translational diffusion D_t of spheres reads $D_t(T) = k_BT/(6\pi\eta R_h)$, where k_B is the Boltzmann constant and R_h the

https://doi.org/10.1021/acs.nanolett.6c01347
Nano Lett. 2026, 26, 8208−8216

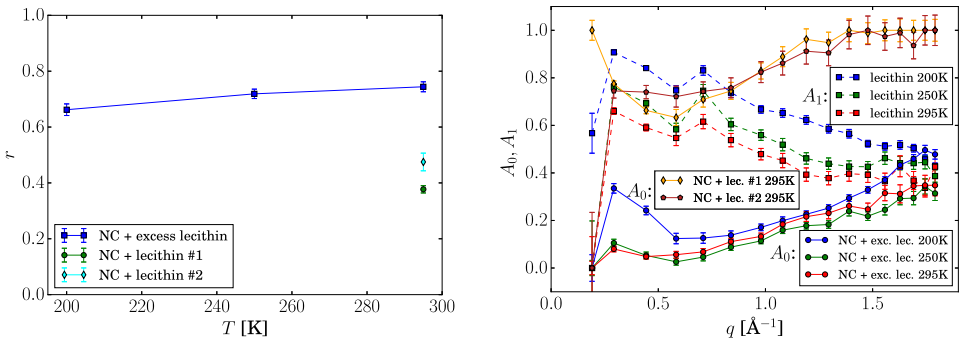

Figure 4. QENS results: Left: Scaling parameter r of the spectral amplitude contributions from the NCs over the lecithin, eq 2. Note that r cannot be associated with the number density ratio of the NCs over micelles, since the signal amplitude depends on the coverage of the NCs as well as on the coverage-dependent dynamic dissociation. Right: Amplitude ratios of the center-of-mass and internal diffusion contributions for the NCs A_0 and lecithin A_1 (eq 2), respectively.

hydrodynamic radius. Assuming $D_{t,\mathrm{LE}} \approx D_{\mathrm{LE}}$ for the lecithin micelles, $R_{h,\mathrm{LE}} = (2.5 \pm 0.03)$nm (fitted solid line on D_{LE} in Figure 3 bottom left). The above expression for the Stokes–Einstein relation neglects a small contribution from the rotational diffusion D_r.[50] Therefore, R_h is underestimated, since the D_t is overestimated by not accounting for D_r, but a quantitive treatment of D_r would require knowledge of the hydrogen density distribution.[50] Crowding and bidispersity in the suspension also affect D_{NC} and D_{LE},[51−54] leading to an overall slowing-down, but speeding-up of the smaller micelles relative to the larger NCs. However, these effects are small given the low total particle volume fraction $\varphi < 0.05$ in all samples. Thus, the micelle radius found from QENS can be considered to be in reasonable agreement with the radius found from SANS.

In contrast to the lecithin micelles, the NCs do not show a temperature-dependence expected for Stokes–Einstein diffusion of particles with a constant size, possibly due to temperature-dependent aggregation. At $T = 295$ K, we find the apparent hydrodynamic radius $R_{h,\mathrm{NC}} = 7.7$ nm in the presence of excess lecithin. $R_{h,\mathrm{NC}}$ is substantially larger than the radius of a single NC concluded from SEM and SAXS/SANS, possibly due to a transient aggregation not visible in the time-average seen by SAXS/SANS.

Next, we address the lateral diffusion of the lecithin relative to the NCs and micelles, respectively. Figure 3 (bottom right) displays D_{jump}, which has to be considered together with its relative amplitudes A_0 and A_1 depicted in Figure 4 (right), attributed to lecithin in micelles and on NCs, respectively (cf. eq 2). The high-q limit of $A_{0,1}(q)$ approximately represents the fraction of hydrogen atoms that are immobile on the nanosecond observation time of the QENS experiment. For the as-synthesized NC samples, $A_0 \approx 1$, i.e., most of the lecithin contributing to the NC signal appears to be tightly attached to the NCs. In contrast, in the presence of excess lecithin, only a small fraction of this lecithin is immobile relative to the NC surface. A_1 associated with the lecithin can be interpreted as the elastic incoherent structure factor, EISF,[55] of lecithin within the micelles (symbols connected by dashed lines in Figure 4, right). In contrast, A_0 cannot be easily understood as an EISF due to its strongly nonmonotonous dependence on q and increase toward high q. The maximum near $q \approx 1.8$Å^{-1} may be associated with strongly localized motions[56] or be a result of an incomplete model scattering function, eq 2.[57] This incompleteness of the model might arise from not accounting for a fraction of completely free lecithin. In a different interpretation, $(1 - A_0(q))$ rather than $A_0(q)$ would be the effective EISF for lecithin relative to the NCs, because this EISF would reflect the dissociation dynamics rather than the lateral diffusion of lecithiun relative to the NCs (Figure S9). In contrast, a confined motion with a confinement length scale commensurate with the q-range accessed would result in a distinct slope change,[58] which we do not see in the EISFs. The mobility inferred from $A_0(q)$ and $A_1(q)$ cannot be directly related to the mobility derived from NMR due to the disparate observation time scales. $D_{\mathrm{jump,NC,LE}}$ are associated with very small residence times $\tau < 12$ ps (eq 3, Figure S10), indicating a nearly Fickian lateral dynamics of lecithin.

$D_{\mathrm{jump,LE}}$ compare reasonably with lateral diffusion in lipid vesicle systems.[43,44] Despite the different observation time scales, our QENS results for $D_{\mathrm{NC,LE}}$ and $D_{\mathrm{jump,NC,LE}}$, respectively, are also broadly consistent with center-of-mass diffusion of NCs inferred earlier from NMR[25,40] as well as with molecular ligand diffusion observed by FCS[59] and in similar NC systems by DOSY NMR.[40]

For completeness, we report the fit parameters $\beta(q)$ and $\gamma_{\mathrm{Tol}}(q)$ in the SI (Figures S11 and S12). $\beta(q)$ represents the thermal Debye–Waller-factor of the system (Figure S11), and the solvent widths γ_{Tol} show de Gennes narrowing[60] expected for coherent scattering (Figure S12).

The scalar r relates the QENS signal amplitudes of lecithin on micelles over lecithin on NCs (eq 2, Figure 4 left). We find that r is larger for the excess lecithin sample than for the as-synthesized samples, which may seem counterintuitive. However, r depends on the coverage by lecithin, and the product $r \cdot A_0$ is smaller for the excess lecithin sample than for the as-synthesized samples.

To further interpret the NMR and QENS results, we consider the NC surface chemistry. We assign the alkene ^{1}H NMR peaks to relatively more weakly and tightly bound ligand species, respectively (Table S2). We tentatively associate the ratio of their peak areas with an equilibrium resulting from the binding of these ligand species. For the excess ligand sample, we observe the highest fraction, and for pure lecithin micelles the lowest fraction of weakly bound lecithin. In the QENS signal, this binding ratio appears to result in a higher apparent fraction of lecithin on NCs over lecithin in micelles. Simultaneously, in this situation more ligand molecules appear to be present in solution, inducing the formation of further micelles.

We propose a simple picture for these two species: Lecithin consists of lipid molecules with zwitterionic head groups,[61]

https://doi.org/10.1021/acs.nanolett.6c01347
Nano Lett. 2026, 26, 8208−8216

corresponding to two functional groups that can bind to a surface, namely the trimethylammonium $N(CH_3)_3^+$ and phosphoric acid groups. The weakly attached species may be a lecithin molecule bound with only one of the respective groups, whereas the tightly bound lecithin would be attached with both groups simultaneously, cf. the schematic in Figure 1(a). When less surface area per ligand is available, more lecithin may be bound with the amine group. This functional group being at a terminal position, the remainder of the molecule must point away from the surface (Figure 1(a), bottom right). In this picture of two possible binding sites per lecithin molecule, the higher area fraction of weakly bound ligand for the excess lecithin sample implies that the addition of more ligand results in more lecithin being weakly attached to the NC surface, i.e., only bound with one functional group. This binding site picture does not conflict with the strong binding of lecithin to lead halide perovskite NCs reported earlier *inter alia* via anion exchange,[40,62] because the mobility observed by QENS agrees with a picture of the lecithin diffusing laterally along the NC and micelle surfaces while maintaining its attachment. Moreover, for the as-synthesized NCs, the signal amplitude $(1 - A_0(q))$ associated with the lateral diffusion is small (eq 2 and Figure 4(right)).

We speculate that the higher decoration of the NCs in the presence of excess ligand results in an increase of the effective ligand shell thickness, because a smaller surface area per ligand is available and the higher coverage may impose a more upright alignment of the lecithin lipid chains. However, D for the decorated NCs in the excess lecithin sample is larger than in the as-synthesized samples (Figure 3, bottom left), suggesting a smaller effective radius $R_{h,NC}$. As a competing effect, the NCs with higher coverage may have a lower tendency to aggregate, explaining the smaller $R_{h,NC}$. This possible coverage-dependent aggregation is not necessarily conclusively visible in SAXS/SANS, since the aggregation may be dynamic or transient, as mentioned earlier. The NC center-of-mass diffusion observed by QENS on the nanosecond time scale confirms their colloidal stability and complements observations made on much longer time scales by DOSY NMR.[40]

In summary, by combining NMR with SAXS/SANS and QENS, we gain knowledge on the surface chemistry and solution structure of L-α-lecithin functionalized $CsPbBr_3$ NCs in liquid toluene suspensions. From SAXS/SANS we find that all samples contain reverse ligand micelles with a radius of approximately 3.0 nm. For both the NCs and micelles, separate center-of-mass diffusion coefficients are observed by QENS. In the as-synthesized samples, the micelle fraction is smaller than in the excess lecithin sample. Additionally, from NMR we infer the presence of different ligand species marked by different bonding strength: Lecithin can be attached by either both of its two functional groups or by only one. Upon increasing the ligand density, the latter case becomes more probable as less surface area per ligand is available. A picture of a dynamic equilibrium emerges, consistent with different bonding strengths seen by NMR and with the lateral diffusion processes on the time scale of the order of 100 ps and apparent EISFs identified by QENS. Even though this lateral diffusion cannot be further dissociated into different dynamic contributions, the nearly unrestricted geometrical character of this diffusion seen in the nearly vanishing residence time and large mean free path seen in the EISF are consistent with this dynamic picture.

In conclusion, lecithin functionalized $CsPbBr_3$ NCs exhibit a dynamic surface equilibrium confirmed by both QENS and NMR, which can be tuned by varying the ligand density via excess lecithin, and which coexists with ligand reverse micelles confirmed by SAXS/SANS. SAXS/SANS and QENS both confirm that the NCs are colloidally stable in d-toluene. However, the center-of-mass diffusion of the NCs indicates the formation of small NCs assemblies, consistent with the incomplete surface coverage suggested by SANS. This work has established the *in situ* combination of SAXS/SANS and of a novel QENS experiment with an optimized observation window for NCs. It may inspire further experiments using neutrons to access the pico- to nanosecond diffusion time scale on the nanometer length scale for organically decorated NCs, and to connect the information on dynamics with information on NC surface and colloidal structure. Future ligand exchange procedures can exploit the tuning of the surface equilibrium, and thus of the binding situation.

MATERIALS AND METHODS

The NC/lecithin samples in d8-toluene were prepared following Krieg et al.[22] as explained in detail in the SI. Two "as-synthesized" NC/lecithin samples from the same batch were measured by QENS and SAXS/SANS, namely 275 mg/mL NCs with 18 mg/mL lecithin and 200 mg/mL NCs with 13 mg/mL lecithin, i.e, at the same lecithin/NC ratio with different dilution, denoted "NC + lecithin #1" and "···#2", respectively, in the QENS figure legends. Only "lecithin #1" was also measured with NMR. One NC with excess lecithin sample (138 mg/mL NCs with 38 mg/mL lecithin) was measured with all methods. While NMR and QENS samples were hermetically sealed, transfer from QENS to SAXS/SANS involved unavoidable exposure to air.

NMR was carried out using a Bruker Avance III HDX 400, simulatenous SAXS/SANS using D22,[17] and QENS using IN16B/BATS at the ILL.[18,19] SAXS/SANS data were analyzed using SASfit.[63] QENS data were reduced using Mantid[64] and fitted using python[65] employing *scipy.optimize.curve_fit*. Further details are reported in the SI.

ASSOCIATED CONTENT

Data Availability Statement

The neutron data are permanently curated by the ILL and accessible under http://doi.ill.fr/10.5291/ILL-DATA.INTER-529.[66]

Supporting Information

The Supporting Information is available free of charge at https://pubs.acs.org/doi/10.1021/acs.nanolett.6c01347.

Detailed materials and methods, additional ^{1}H NMR spectra and fit parameters, UV−vis spectra, SEM images, photoluminescence spectra, SAXS/SANS curves, details of the QENS fitting procedure, additional QENS spectra and QENS fit parameters, and DLS results (PDF)

AUTHOR INFORMATION

Corresponding Author

Tilo Seydel − *Institut Max von Laue - Paul Langevin, F-38000 Grenoble, France;* orcid.org/0000-0001-9630-1630; Email: seydel@ill.eu

Authors

Jan Wahl − *Institut für Physikalische und Theoretische Chemie, Universität Tübingen, D-72076 Tübingen, Germany*

https://doi.org/10.1021/acs.nanolett.6c01347
Nano Lett. 2026, 26, 8208−8216

Ivan Zaluzhnyy − *Institut für Angewandte Physik, Universität Tübingen, D-72076 Tübingen, Germany; Center for Light-Matter Interaction, Sensors & Analytics LISA+, Universität Tübingen, D-72076 Tübingen, Germany;* orcid.org/0000-0001-5946-2777

Sylvain Prevost − *Institut Max von Laue - Paul Langevin, F-38000 Grenoble, France*

Lionel Porcar − *Institut Max von Laue - Paul Langevin, F-38000 Grenoble, France*

Christian Beck − *Institut für Angewandte Physik, Universität Tübingen, D-72076 Tübingen, Germany; Institut Max von Laue - Paul Langevin, F-38000 Grenoble, France;* Present Address: European Spallation Source ERIC, Data Management and Scientific Computing Centre, Asmussens Allé Bygning 305, 2800 Lyngby, Denmark; orcid.org/0000-0001-7214-3447

Olga Matsarskaia − *Institut Max von Laue - Paul Langevin, F-38000 Grenoble, France;* orcid.org/0000-0002-7293-7287

Tobias Unruh − *Institut für Physik der Kondensierten Materie, Universität Erlangen-Nürnberg, D-91058 Erlangen, Germany;* orcid.org/0000-0002-8903-4850

Ezzeldin Metwalli − *Institut für Physik der Kondensierten Materie, Universität Erlangen-Nürnberg, D-91058 Erlangen, Germany;* Present Address: Faculty of Engineering and Materials Science, German University in Cairo, Cairo, Egypt.; orcid.org/0000-0003-2642-5130

Frank Schreiber − *Institut für Angewandte Physik, Universität Tübingen, D-72076 Tübingen, Germany; Center for Light-Matter Interaction, Sensors & Analytics LISA+, Universität Tübingen, D-72076 Tübingen, Germany;* orcid.org/0000-0003-3659-6718

Marcus Scheele − *Institut für Physikalische und Theoretische Chemie, Universität Tübingen, D-72076 Tübingen, Germany; Center for Light-Matter Interaction, Sensors & Analytics LISA+, Universität Tübingen, D-72076 Tübingen, Germany;* orcid.org/0000-0002-2704-3591

Complete contact information is available at: https://pubs.acs.org/10.1021/acs.nanolett.6c01347

Author Contributions

J.W. prepared the samples and performed the SEM, UV−vis and NMR experiments; I.Z. performed the DLS experiment; C.B. and T.S. performed the QENS experiment; S.P., L.P., E.M., O.M. and T.U. performed the SAXS/SANS experiment; S.P. and J.W. analyzed the SAXS/SANS data; J.W. and T.S. analyzed the NMR data; T.S. analyzed the QENS data; M.S., F.S., T.U., and T.S. designed the research; all authors contributed to interpreting the results and writing the manuscript.

Notes

The authors declare no competing financial interest.

■ ACKNOWLEDGMENTS

We acknowledge funding by the DFG under grants SCHE1905/8-1 (project no. 424708673), SCHR700/47-1 and SCHE1905/9-1, as well as by the BMBF for the BATS mode of IN16B (ErUM-pro 05K19VTB and 05K22VTA), and for the simultaneous SAXS/SANS setup on D22 (ErUM-pro 05K16WE1). C.B. acknowledges a postdoctoral fellowship funded by the BMBF (ErUM-pro 05K19VTB and 05K22VTA). We acknowledge the allocation of internal beam time by the ILL while the COVID-19 pandemic was still ongoing in March 2021.

■ REFERENCES

(1) Quan, L. N.; Rand, B. P.; Friend, R. H.; Mhaisalkar, S. G.; Lee, T.-W.; Sargent, E. H. Perovskites for next-generation optical sources. *Chem. Rev.* **2019**, *119* (12), 7444−7477.

(2) Protesescu, L.; Yakunin, S.; Bodnarchuk, M. I.; Krieg, F.; Caputo, R.; Hendon, C. H.; Yang, R. X.; Walsh, A.; Kovalenko, M. V. Nanocrystals of cesium lead halide perovskites ($CsPbX_3$, X= Cl, Br, and I): novel optoelectronic materials showing bright emission with wide color gamut. *Nano Lett.* **2015**, *15* (6), 3692−3696.

(3) Kovalenko, M. V.; Manna, L.; Cabot, A.; Hens, Z.; Talapin, D. V.; Kagan, C. R.; Klimov, V. I.; Rogach, A. L.; Reiss, P.; Milliron, D. J.; et al. Prospects of nanoscience with nanocrystals. *ACS Nano* **2015**, *9* (2), 1012−1057.

(4) Hills-Kimball, K.; Yang, H.; Cai, T.; Wang, J.; Chen, O. Recent advances in ligand design and engineering in lead halide perovskite nanocrystals. *Advanced Science* **2021**, *8* (12), 2100214.

(5) Hiller, J. L.; Thalwitzer, R.; Bozkurt, A.; Ferreira, M. G.; Hodak, R.; Strauß, F.; Nadler, E.; Hinsley, G. N.; Wang, B.; Ngoi, K. H.; Rudzinski, W.; Kneschaurek, E.; Roseker, W.; Sprung, M.; Lapkin, D.; Baranov, D.; Schreiber, F.; Vartanyants, I. A.; Scheele, M.; Zaluzhnyy, I. A. Mechanically robust supercrystals from antisolvent-induced assembly of perovskite nanocrystals. *ACS Nano* **2025**, *19* (28), 26117−26126.

(6) Krieg, F.; Ochsenbein, S. T.; Yakunin, S.; Ten Brinck, S.; Aellen, P.; Süess, A.; Clerc, B.; Guggisberg, D.; Nazarenko, O.; Shynkarenko, Y.; et al. Colloidal $CsPbX_3$ (X= Cl, Br, I) nanocrystals 2.0: Zwitterionic capping ligands for improved durability and stability. *ACS Energy Letters* **2018**, *3* (3), 641−646.

(7) Wang, H.; Zhang, X.; Sui, N.; Hu, Y.; Colvin, V. L.; Yu, W. W.; Zhang, Y. Photoluminescence loss and recovery of α-CsPbI3 quantum dots originated from chemical equilibrium shift of oleylammonium. *ACS Appl. Mater. Interfaces* **2020**, *12* (10), 11769−11777.

(8) Chen, J.; Chen, S.; Liu, X.; Zhu, D.; Cai, B.; Luo, X.; Feng, W.; Cheng, Y.; Xiong, Y.; Du, J.; et al. Molecule-induced ripening control in perovskite quantum dots for efficient and stable light-emitting diodes. *Science Advances* **2025**, *11* (11), No. eads7159.

(9) Wahl, J.; Engelmayer, M.; Mandal, M.; Naujoks, T.; Haizmann, P.; Maier, A.; Peisert, H.; Andrienko, D.; Brütting, W.; Scheele, M. Porphyrin functionalization of $CsPbBrI_2/SiO_2$ core−shell nanocrystals enhances the stability and efficiency in electroluminescent devices. *Advanced Optical Materials* **2022**, *10* (4), 2101945.

(10) Zhao, L.; Yeh, Y.-W.; Tran, N. L.; Wu, F.; Xiao, Z.; Kerner, R. A.; Lin, Y. L.; Scholes, G. D.; Yao, N.; Rand, B. P. In situ preparation of metal halide perovskite nanocrystal thin films for improved light-emitting devices. *ACS Nano* **2017**, *11* (4), 3957−3964.

(11) Tan, Y.; Zou, Y.; Wu, L.; Huang, Q.; Yang, D.; Chen, M.; Ban, M.; Wu, C.; Wu, T.; Bai, S.; et al. Highly luminescent and stable perovskite nanocrystals with octylphosphonic acid as a ligand for efficient light-emitting diodes. *ACS Appl. Mater. Interfaces* **2018**, *10* (4), 3784−3792.

(12) Wahl, J.; Haizmann, P.; Kirsch, C.; Frecot, R.; Mukharamova, N.; Assalauova, D.; Kim, Y. Y.; Zaluzhnyy, I.; Chassé, T.; Vartanyants, I. A.; et al. Mitigating the photodegradation of all-inorganic mixed-halide perovskite nanocrystals by ligand exchange. *Phys. Chem. Chem. Phys.* **2022**, *24* (18), 10944−10951.

(13) Grisorio, R.; Di Clemente, M. E.; Fanizza, E.; Allegretta, I.; Altamura, D.; Striccoli, M.; Terzano, R.; Giannini, C.; Irimia-Vladu, M.; Suranna, G. P. Exploring the surface chemistry of cesium lead halide perovskite nanocrystals. *Nanoscale* **2019**, *11* (3), 986−999.

(14) Van Zijl, P.; MacLean, C.; Bothner-By, A. Angular correlation and diamagnetic susceptibilities studied by high field NMR. *J. Chem. Phys.* **1985**, *83* (9), 4410−4417.

(15) Fujara, F.; Wefing, S.; Spiess, H. Dynamics of molecular reorientations: Analogies between quasielastic neutron scattering and deuteron NMR spin alignment. *J. Chem. Phys.* **1986**, *84* (8), 4579−4584.

(16) Van Hove, L. Correlations in space and time and Born approximation scattering in systems of interacting particles. *Phys. Rev.* **1954**, *95* (1), 249.
(17) Metwalli, E.; Götz, K.; Lages, S.; Bär, C.; Zech, T.; Noll, D. M.; Schuldes, I.; Schindler, T.; Prihoda, A.; Lang, H.; Grasser, J.; Jacques, M.; Didier, L.; Cyril, A.; Martel, A.; Porcar, L.; Unruh, T. A novel experimental approach for nanostructure analysis: simultaneous small-angle X-ray and neutron scattering. *J. Appl. Crystallogr.* **2020**, *53*, 722−733.
(18) Frick, B.; Mamontov, E.; Eijck, L. v.; Seydel, T. Recent backscattering instrument developments at the ILL and SNS. *Zeitschrift für physikalische Chemie* **2010**, *224* (1−2), 33−60.
(19) van Eijck, L.; Gérard, L.; Frick, B.; Seydel, T.; Schober, H. A case study for using neutron backscattering instruments at reactors in inverted time-of-flight mode. *Nuclear Instruments and Methods in Physics Research Section A: Accelerators, Spectrometers, Detectors and Associated Equipment* **2012**, *672*, 64−68.
(20) Appel, M.; Frick, B.; Magerl, A. A flexible high speed pulse chopper system for an inverted neutron time-of-flight option on backscattering spectrometers. *Sci. Rep.* **2018**, *8* (1), 13580.
(21) Seydel, T.; Koza, M. M.; Matsarskaia, O.; André, A.; Maiti, S.; Weber, M.; Schweins, R.; Prévost, S.; Schreiber, F.; Scheele, M. A neutron scattering perspective on the structure, softness and dynamics of the ligand shell of PbS nanocrystals in solution. *Chemical Science* **2020**, *11* (33), 8875−8884.
(22) Krieg, F.; Ong, Q. K.; Burian, M.; Rainò, G.; Naumenko, D.; Amenitsch, H.; Süess, A.; Grotevent, M. J.; Krumeich, F.; Bodnarchuk, M. I.; et al. Stable ultraconcentrated and ultradilute colloids of $CsPbX_3$ (X= Cl, Br) nanocrystals using natural lecithin as a capping ligand. *J. Am. Chem. Soc.* **2019**, *141* (50), 19839−19849.
(23) Brus, L. Electronic wave functions in semiconductor clusters: experiment and theory. *J. Phys. Chem.* **1986**, *90* (12), 2555−2560.
(24) Fritzinger, B.; Capek, R. K.; Lambert, K.; Martins, J. C.; Zeger, H. Utilizing self-exchange to address the binding of carboxylic acid ligands to CdSe quantum dots. *J. Am. Chem. Soc.* **2010**, *132* (29), 10195−10201.
(25) De Roo, J.; Yazdani, N.; Drijvers, E.; Lauria, A.; Maes, J.; Owen, J. S.; Van Driessche, I.; Niederberger, M.; Wood, V.; Martins, J. C.; Zeger, H.; et al. Probing solvent−ligand interactions in colloidal nanocrystals by the NMR line broadening. *Chem. Mater.* **2018**, *30* (15), 5485−5492.
(26) Wu, M.; Vartanian, A. M.; Chong, G.; Pandiakumar, A. K.; Hamers, R. J.; Hernandez, R.; Murphy, C. J. Solution NMR analysis of ligand environment in quaternary ammonium-terminated self-assembled monolayers on gold nanoparticles: the effect of surface curvature and ligand structure. *J. Am. Chem. Soc.* **2019**, *141* (10), 4316−4327.
(27) Higinbotham, J.; Marshall, I. NMR lineshapes and lineshape fitting procedures. *Annu. Rep. NMR Spectrosc.* **2001**, *43*, 59−120.
(28) Sarkar, D.; Stelmakh, A.; Karmakar, A.; Aebli, M.; Krieg, F.; Bhattacharya, A.; Pawsey, S.; Kovalenko, M. V.; Michaelis, V. K. Surface structure of lecithin-capped cesium lead halide perovskite nanocrystals using solid-state and dynamic nuclear polarization NMR spectroscopy. *ACS Nano* **2024**, *18* (33), 21894−21910.
(29) Levy, R. M.; Karplus, M.; Wolynes, P. G. NMR relaxation parameters in molecules with internal motion: exact Langevin trajectory results compared with simplified relaxation models. *J. Am. Chem. Soc.* **1981**, *103* (20), 5998−6011.
(30) Vogel, M. NMR studies on simple liquids in confinement. *European Physical Journal Special Topics* **2010**, *189* (1), 47−64.
(31) Kumar, G. A.; McAllister, M. A. Theoretical investigation of the relationship between proton NMR chemical shift and hydrogen bond strength. *Journal of Organic Chemistry* **1998**, *63* (20), 6968−6972.
(32) Hiller, J. L.; Thalwitzer, R.; Bozkurt, A.; Carter, R. E.; Hettiger, T.; Fröhlich, M.; Hodak, R.; Ferreira, M. G.; Eberle, M.; Kneschaurek, E.; et al. How antisolvent-induced ligand stripping shapes $CsPbX_3$ nanocrystals and their assemblies. *Nano Lett.* **2026**, *26* (8), 2955−2963.
(33) Schurtenberger, P.; Scartazzini, R.; Magid, L. J.; Leser, M. E.; Luisi, P. L. Structural and dynamic properties of polymer-like reverse micelles. *J. Phys. Chem.* **1990**, *94* (9), 3695−3701.
(34) Bradley-Shaw, J. L.; Camp, P. J.; Dowding, P. J.; Lewtas, K. Glycerol monooleate reverse micelles in nonpolar solvents: Computer simulations and small-angle neutron scattering. *J. Phys. Chem. B* **2015**, *119* (11), 4321−4331.
(35) Walde, P.; Giuliani, A. M.; Boicelli, C.; Luisi, P. L. Phospholipid-based reverse micelles. *Chem. Phys. Lipids* **1990**, *53* (4), 265−288.
(36) Willard, D. M.; Riter, R. E.; Levinger, N. E. Dynamics of polar solvation in lecithin/water/cyclohexane reverse micelles. *J. Am. Chem. Soc.* **1998**, *120* (17), 4151−4160.
(37) Maier, A.; Lapkin, D.; Mukharamova, N.; Frech, P.; Assalauova, D.; Ignatenko, A.; Khubbutdinov, R.; Lazarev, S.; Sprung, M.; Laible, F.; Löffler, R.; Previdi, N.; Bräuer, A.; Günkel, T.; Fleischer, M.; Schreiber, F.; Vartanyants, I. A.; Scheele, M. Structure−transport correlation reveals anisotropic charge transport in coupled pbs nanocrystal superlattices. *Adv. Mater.* **2020**, *32* (36), 2002254.
(38) Sears, V. Scattering lengths for neutrons. In *International Tables for Crystallography Volume C*; Wiley: 2006; Vol. *4.4*, pp 444−454
(39) Wiedenmann, A.; Keiderling, U.; Habicht, K.; Russina, M.; Gähler, R. Dynamics of field-induced ordering in magnetic colloids studied by new time-resolved small-angle neutron-scattering techniques. *Phys. Rev. Lett.* **2006**, *97*, 057202.
(40) Berezovska, Y.; Sabisch, S.; Bernasconi, C.; Sahin, Y.; Bertolotti, F.; Guagliardi, A.; Bodnarchuk, M. I.; Dirin, D. N.; Kovalenko, M. V. Tightly yet dynamically bound aliphatic guanidinium ligands for lead halide perovskite nanocrystals. *J. Am. Chem. Soc.* **2025**, *147* (39), 35446−35455.
(41) Qvist, J.; Schober, H.; Halle, B. Structural dynamics of supercooled water from quasielastic neutron scattering and molecular simulations. *J. Chem. Phys.* **2011**, *134* (14), 144508.
(42) Ahmadi, D.; Thompson, K. C.; García Sakai, V.; Schweins, R.; Moulin, M.; Haertlein, M.; Strohmeier, G. A.; Pichler, H.; Forsyth, V. T.; Barlow, D. J.; et al. Nanoscale structure and dynamics of model membrane lipid raft systems, studied by neutron scattering methods. *Frontiers in Physics* **2022**, *10*, 864746.
(43) Sharma, V.; Srinivasan, H.; Gupta, J.; Mitra, S. Lipid lateral diffusion: mechanisms and modulators. *Soft Matter* **2024**, *20* (39), 7763−7796.
(44) Busch, S.; Smuda, C.; Pardo, L. C.; Unruh, T. Molecular mechanism of long-range diffusion in phospholipid membranes studied by quasielastic neutron scattering. *J. Am. Chem. Soc.* **2010**, *132* (10), 3232−3233.
(45) Singwi, K.; Sjölander, A. Diffusive motions in water and cold neutron scattering. *Phys. Rev.* **1960**, *119* (3), 863.
(46) Artaki, I.; Jonas, J. Pressure effect on the coupling between rotational and translational motions of supercooled viscous fluids. *J. Chem. Phys.* **1985**, *82* (7), 3360−3370.
(47) Evans, R.; Deng, Z.; Rogerson, A. K.; McLachlan, A. S.; Richards, J. J.; Nilsson, M.; Morris, G. A. Quantitative interpretation of diffusion-ordered NMR spectra: can we rationalize small molecule diffusion coefficients. *Angew. Chem., Int. Ed* **2013**, *52* (11), 3199−3202.
(48) Wilbur, D. J.; Jonas, J. Fourier transform NMR in liquids at high pressure. III. Spin−lattice relaxation in toluene-d8. *J. Chem. Phys.* **1975**, *62* (7), 2800−2807.
(49) Einstein, A. Über die von der molekularkinetischen Theorie der Wärme geforderte Bewegung von in ruhenden Flüssigkeiten suspendierten Teilchen. *Annalen der Physik* **1905**, *322* (8), 549−560.
(50) Grimaldo, M.; Roosen-Runge, F.; Jalarvo, N.; Zamponi, M.; Zanini, F.; Hennig, M.; Zhang, F.; Schreiber, F.; Seydel, T. High-resolution neutron spectroscopy on protein solution samples. In *EPJ. Web of Conferences*; EDP Sciences: 2015; Vol. *83*, p 02005.
(51) Beck, C.; Grimaldo, M.; Lopez, H.; Da Vela, S.; Sohmen, B.; Zhang, F.; Oettel, M.; Barrat, J.-L.; Roosen-Runge, F.; Schreiber, F.; et al. Short-time transport properties of bidisperse suspensions of

https://doi.org/10.1021/acs.nanolett.6c01347
Nano Lett. 2026, 26, 8208−8216

immunoglobulins and serum albumins consistent with a colloid physics picture. *J. Phys. Chem. B* **2022**, *126* (38), 7400−7408.
(52) Wang, M.; Brady, J. F. Short-time transport properties of bidisperse suspensions and porous media: A Stokesian dynamics study. *J. Chem. Phys.* **2015**, *142* (9), 094901.
(53) Banchio, A. J.; Nägele, G. Short-time transport properties in dense suspensions: From neutral to charge-stabilized colloidal spheres. *J. Chem. Phys.* **2008**, *128* (10), 104903.
(54) Nägele, G. On the dynamics and structure of charge-stabilized suspensions. *Phys. Rep.* **1996**, *272* (5−6), 215−372.
(55) Bée, M. A physical insight into the elastic incoherent structure factor. *Physica B: Condensed Matter* **1992**, *182* (4), 323−336.
(56) Jacobsen, J.; Rodrigues, M. S.; Telling, M. T.; Beraldo, A. L.; Santos, S. F.; Aldridge, L. P.; Bordallo, H. N. Nano-scale hydrogen-bond network improves the durability of greener cements. *Sci. Rep.* **2013**, *3* (1), 2667.
(57) Michot, L. J.; Delville, A.; Humbert, B.; Plazanet, M.; Levitz, P. Diffusion of water in a synthetic clay with tetrahedral charges by combined neutron time-of-flight measurements and molecular dynamics simulations. *J. Phys. Chem. C* **2007**, *111* (27), 9818−9831.
(58) Volino, F.; Dianoux, A. Neutron incoherent scattering law for diffusion in a potential of spherical symmetry: general formalism and application to diffusion inside a sphere. *Mol. Phys.* **1980**, *41* (2), 271−279.
(59) Andrews, A. B.; Guerra, R. E.; Mullins, O. C.; Sen, P. N. Diffusivity of asphaltene molecules by fluorescence correlation spectroscopy. *J. Phys. Chem. A* **2006**, *110* (26), 8093−8097.
(60) De Gennes, P. Liquid dynamics and inelastic scattering of neutrons. *Physica* **1959**, *25* (7−12), 825−839.
(61) List, G. 1 - soybean lecithin: Food, industrial uses, and other applications. In *Polar Lipids*; Ahmad, M. U., Xu, X., Eds.; Elsevier: 2015; pp 1−33, .
(62) Scharf, E.; Krieg, F.; Elimelech, O.; Oded, M.; Levi, A.; Dirin, D. N.; Kovalenko, M. V.; Banin, U. Ligands mediate anion exchange between colloidal lead-halide perovskite nanocrystals. *Nano Lett.* **2022**, *22* (11), 4340−4346.
(63) Breßler, I.; Kohlbrecher, J.; Thünemann, A. F. SASfit: a tool for small-angle scattering data analysis using a library of analytical expressions. *J. Appl. Crystallogr.* **2015**, *48* (5), 1587−1598.
(64) Arnold, O.; Bilheux, J.-C.; Borreguero, J.; Buts, A.; Campbell, S. I.; Chapon, L.; Doucet, M.; Draper, N.; Leal, R. F.; Gigg, M.; et al. Mantid-data analysis and visualization package for neutron scattering and μ SR experiments. *Nuclear Instruments and Methods in Physics Research Section A: Accelerators, Spectrometers, Detectors and Associated Equipment* **2014**, *764*, 156−166.
(65) Beck, C.; Pounot, K.; Mosca, I.; Jalarvo, N. H.; Roosen-Runge, F.; Schreiber, F.; Seydel, T. Notes on fitting and analysis frameworks for QENS spectra of (soft) colloid suspensions. In *EPJ. Web of Conferences*; EDP Sciences: 2022; Vol. *272*, p 01004
(66) Wahl, J.; Seydel, T. Data from Diffuse ligand dynamics in colloidal suspensions of lead halide perovskite nanocrystals; *ILL data, Institut Laue-Langevin (ILL)*, 2021. DOI: 10.5291/ILL-DATA.-INTER-529.

https://doi.org/10.1021/acs.nanolett.6c01347
Nano Lett. 2026, 26, 8208−8216